Exploration Geophysics (2004) ***35****, 297-305*

GETMAG – a SQUID magnetic tensor gradiometer for mineral and oil exploration

Phillip Schmidt[1] **David Clark** **Keith Leslie** **Marcel Bick** **David Tilbrook** **Cathy Foley**

Key Words: gradiometer, tensor, SQUID, Fourier, Euler

ABSTRACT

A novel rotating magnetic gradiometer system (GETMAG) has been designed, constructed, and demonstrated. The sensor is a high temperature superconducting quantum interference device (SQUID) operating in liquid nitrogen (-196°C). By making measurements about three separate axes, the full magnetic gradient tensor is determined.

The system has been demonstrated over a magnetite skarn deposit at Tallawang, near Gulgong, NSW, which is essentially two-dimensional (2D). The 2D structure was important because it allowed an unaliased total magnetic intensity (TMI) survey to be carried out in parallel, from which tensor components could be calculated to directly compare with the tensor components measured with the rotating gradiometer. The agreement was found to be excellent, confirming the accuracy and calibration of GETMAG and the Fourier filtering method of the calculation.

Methods developed to analyse 2D tensor data utilise eigenvalue and eigenvector systematics. Notwithstanding underlying non-uniqueness of solutions for 2D structures, all determinable parameters of location, geometry, and magnetization were found to accord with directly measured properties, i.e., information gained from either exploration drilling or laboratory measurements. Only a few tensor gradiometer stations were needed to extract the same information as a whole TMI survey.

A more general method to determine structure and location of sources is Tensor Euler Deconvolution. This method has been adapted for the magnetic gradient tensor in a least-squares fashion and applied to the tensors calculated from the TMI survey. Generally, an Euler index of $n = 1$ was found, as is expected for 2D sources. However, this approach allowed second-order features of the source, where $n > 1$, to be discerned. The skarn is interpreted to comprise a fresh, more highly magnetic, core at depth (~25–30 m) surrounded by a less magnetic mantle. The skarn extends to within 10 m of the surface where weathering has presumably contributed to diminished magnetization. Elsewhere, away from the skarn, Euler indices are low, approaching that of a magnetic annihilator ($n = 0$). This presumably reflects the uniformly magnetized alluvial soil cover.

Our next stage is to demonstrate an airborne capability of GETMAG, beginning with a helicopter platform before moving to fixed-wing. In addition to mineral and oil exploration, we envisage applications in environmental, military, and unexploded ordnance (UXO) surveys.

CSIRO Industrial Physics, PO Box 218, Lindfield
NSW, Australia, 2070
Tel: (+612) 9413 7356
Fax: (+612) 9413 7810
[1] *Email: phil.schmidt@csiro.au*

Paper presented at the 17th ASEG Geophysical Conference & Exhibition, August 2004.
Revised manuscript received 28 October, 2004.

INTRODUCTION

Over the past few years, there have been many discussions on the advantages of magnetic gradient tensor surveys as compared to conventional total magnetic intensity (TMI) surveys in mineral and oil exploration (Christensen and Rajagopalan, 2000; Schmidt and Clark, 2000; Heath et al., 2003). If vector information could be retrieved, either by direct measurement or by mathematical manipulation, interpretation of magnetic surveys could be improved to allow for cases where the normal assumptions that attend TMI analyses are violated.

Vector surveys, where the direct measurement of vector components has been attempted, have met with mixed success. The accuracy of direct measurement of the field vector is mostly governed by orientation errors, which for airborne platforms are so large that the theoretical derivation of the vector components from the TMI is actually preferable. For this reason and others listed below, it is desirable to measure the field gradient, rather than field vector.

Gradient measurements are relatively insensitive to orientation. This is because gradients arise largely from anomalous sources, and the background geomagnetic gradient is low. This contrasts with the field vector, which is dominated by the background field from Earth's core.

Gradient measurements are, therefore, most appropriate for airborne applications. Another advantage is that they obviate the need for base stations and corrections for diurnal variations. They also greatly reduce the need for regional corrections, which are required by TMI surveys because of deeper crustal fields that are not of exploration interest, or the normal (quasi-)latitudinal intensity variation of the global field.

Gradient measurements also provide valuable additional information, compared to conventional total-field measurements, when the field is undersampled. Undersampling is common perpendicular to flight lines in airborne surveys, is also a normal feature of ground surveys, and is always a problem with down-hole surveys. Synergistic interpretation of calculated vectors and measured gradients allows significantly more information to be extracted from airborne surveys.

Christensen and Rajagopalan (2000) give two examples where measurement of the anomalous field vector is critical. One of these is for an anomalous field large enough to significantly deflect the resultant field away from the unperturbed local field direction, and the other is in low magnetic latitudes, where anomalies are laterally displaced from their sources and TMI measurements are insensitive to N-S striking structures, thereby greatly complicating interpretation. In both situations, if the anomalous magnetic vector was known rather than just the TMI, then interpretation would be simplified. However, because the measurement of vectors is extremely sensitive to orientation using conventional magnetometers, Christensen and Rajagopalan (2000) conclude that the gradient tensor should be measured. Rajagopalan (pers. comm., 2000) has pointed out the utility of the analytic signal

calculated from the vertical field component, which requires knowledge of three elements of the gradient tensor.

Schmidt and Clark (2000) argued along the same lines suggesting that high-temperature superconducting quantum interference devices (SQUIDs) were the sensors of choice for detecting gradients. These authors also note that the magnetic gradient tensor is admirably suited to environmental applications, for defence purposes such as submarine and unexploded ordnance (UXO) detection and, ultimately, as a down-hole tool.

From theoretical considerations some of the advantages of measuring gradients, particularly the gradient tensor, include:

- Tensor elements are true potential fields with desirable mathematical properties,
- The gradient tensor defines the direction to a compact source directly from measurements at as few as one or two stations,
- The gradient tensor enables direct calculation of the magnetic moment of a compact source,
- Gradient measurements, particularly full tensor measurements, determine on which side of a flight line or a drill hole a source lies,
- Gradient measurements, particularly full tensor measurements, retain the benefits of vector surveys without extreme orientation sensitivity,
- Gradient measurements ensure common-mode rejection of the field from Earth's core, regional fields from the deep crust and geomagnetic variations from the ionosphere and magnetosphere and
- Gradients give better resolution of shallow features and closely spaced sources.

The purpose of this paper is to describe measurement of the magnetic gradient tensor, and to demonstrate the above advantages.

PROPERTIES OF THE MAGNETIC GRADIENT TENSOR

The gradient tensor is a 3 × 3 second-order tensor:

$$\begin{bmatrix} \frac{\partial B_x}{\partial x} & \frac{\partial B_x}{\partial y} & \frac{\partial B_x}{\partial z} \\ \frac{\partial B_y}{\partial x} & \frac{\partial B_y}{\partial y} & \frac{\partial B_y}{\partial z} \\ \frac{\partial B_z}{\partial x} & \frac{\partial B_z}{\partial y} & \frac{\partial B_z}{\partial z} \end{bmatrix} \tag{1}$$

where x, y, and z refer to an orthogonal coordinate system and $\mathbf{B} = (B_x, B_y, B_z)$ denotes the magnetic field and its vector components. In practice, we only need to know five of the elements because essentially both the divergence and the curl of the field are zero so that the tensor is symmetric and traceless (Vrba, 1996).

ANALYSIS OF THE MAGNETIC GRADIENT TENSOR

For isolated dipoles, which are frequently encountered in environmental and defence applications and also provide a good representation of compact geological sources such as iron ore-copper-gold (IOCG) deposits or alteration zones, a number of analytical inversion algorithms for the magnetic gradient tensor are available (Frahm, 1972; Wynn et al., 1975; Wilson, 1985). Of these, the algorithm developed by Wilson (1985) is most easily implemented, although for any of the algorithms, there is four-fold ambiguity in the solutions because the same magnetic gradient tensor results from multiple locations and polarities. There are generally three 'ghost solutions' and one real solution. Depending on the application, whether post-processing a geophysical survey or tracking a dipole source in real-time, the ambiguities can be handled in a number of ways. Since two of the possible solutions are above the observer and two are below, if it is known that the source is above or below then the ambiguity is immediately halved. Also, as mentioned above, if the components of the anomalous field can be determined, either through measurement or calculation from the TMI, a unique solution can be found directly. Indeed, only the signs of the anomalous components are required to eliminate the ambiguity. Otherwise, successive observations, either temporal or spatial, allow the real solution to be separated from the ghost solutions.

From Wilson (1985), the method to determine the source location and moment parameters from the eigenvectors and eigenvalues of the tensor is as follows:

Determine eigenvalues λ_1, λ_2, λ_3 such that λ_3 has the smallest absolute value.

Calculate eigenvectors **u** and **v** corresponding to λ_1 and λ_2.

Depending on eigenvalues, do one of the following:

if $\lambda_3 = \lambda_2 = \lambda_1/2$ then solutions are given by:

$$\hat{\mathbf{n}}_1 = \hat{\mathbf{u}}, \quad \hat{\mathbf{m}}_1 = \mathrm{sgn}(\lambda_3)\hat{\mathbf{u}}, \quad \mu = |\lambda_3|, \quad \text{and} \tag{2}$$

$$\hat{\mathbf{n}}_2 = -\hat{\mathbf{u}}, \quad \hat{\mathbf{m}}_2 = -\mathrm{sgn}(\lambda_3)\hat{\mathbf{u}}, \quad \mu = |\lambda_3|, \tag{3}$$

where **n** and **m** give the direction from the source to the observation station and the direction of the magnetic moment respectively, $\mu = 3M/r^4$ is the reduced magnetic moment, and sgn is the signum function that assigns the sign of a (non-zero) number to a number.

if $\lambda_3 = \lambda_1 = \lambda_2/2$, then solutions are given by:

$$\hat{\mathbf{n}}_1 = \hat{\mathbf{v}}, \quad \hat{\mathbf{m}}_1 = \mathrm{sgn}(\lambda_3)\hat{\mathbf{v}}, \quad \mu = |\lambda_3|, \quad \text{and} \tag{4}$$

$$\hat{\mathbf{n}}_2 = -\hat{\mathbf{v}}, \quad \hat{\mathbf{m}}_2 = -\mathrm{sgn}(\lambda_3)\hat{\mathbf{v}}, \quad \mu = |\lambda_3|. \tag{5}$$

Solutions (2), (3) and (4), (5) are degenerate in that there is only two-fold ambiguity. They correspond to the rare situation where the direction to the source and the direction of the magnetic moment are either parallel or anti-parallel.

Otherwise, $|\lambda_3| < |\lambda_1|$ and $|\lambda_3| < |\lambda_2|$, in which case:

$$\mu = \sqrt{Q^2/2 - 2\lambda_3^2}, \quad \text{where } Q^2 = \lambda_1^2 + \lambda_2^2 + \lambda_3^2, \tag{6}$$

$$\cos(\phi) = \lambda_3/\mu \tag{7}$$

$$\cos(\theta) = \frac{\sin(\phi)}{\sqrt{\left(\alpha_1 + 2\cos(\phi)\right)^2 + \sin^2(\phi)}}, \quad \text{where } \alpha_1 = \lambda_1/\mu. \tag{8}$$

Four possible solutions are:

$$\hat{\mathbf{n}}_1 = \cos(\theta)\hat{\mathbf{u}} + \sin(\theta)\hat{\mathbf{v}} \tag{9}$$

$$\begin{aligned}\hat{\mathbf{m}}_1 = &\left[\cos(\phi)\cos(\theta) - \sin(\phi)\sin(\theta)\right]\hat{\mathbf{u}} \\ &+\left[\cos(\phi)\sin(\theta) + \sin(\phi)\cos(\theta)\right]\hat{\mathbf{v}}\end{aligned} \tag{10}$$

$$\hat{\mathbf{n}}_2 = -\hat{\mathbf{n}}_1 \tag{11}$$

$$\hat{\mathbf{m}}_2 = -\hat{\mathbf{m}}_1 \tag{12}$$

$$\hat{\mathbf{n}}_3 = \cos(\theta)\hat{\mathbf{u}} - \sin(\theta)\hat{\mathbf{v}} \tag{13}$$

$$\begin{aligned}\hat{\mathbf{m}}_3 = &\left[\cos(\phi)\cos(\theta) + \sin(\phi)\sin(\theta)\right]\hat{\mathbf{u}} \\ &+\left[\cos(\phi)\sin(\theta) - \sin(\phi)\cos(\theta)\right]\hat{\mathbf{v}}\end{aligned} \tag{14}$$

$$\hat{\mathbf{n}}_4 = -\hat{\mathbf{n}}_3 \tag{15}$$

$$\hat{\mathbf{m}}_4 = -\hat{\mathbf{m}}_3 \tag{16}$$

This algorithm has been tested using a synthetic example where the tensor has been analytically calculated. In the following example, the sources are two spheres based on the sphere model described by Emerson et al. (1985). The results are plotted in Figure 1, which shows the vectors towards the sources and reduced magnetic moments projected onto the horizontal and vertical planes. Only solutions for which the absolute magnitude of the eigenvalues exceeds some pre-determined threshold are plotted. It is clear that the two sources are well located and the directions of the magnetic moments (declination = 330°, inclination = -45°) are well determined.

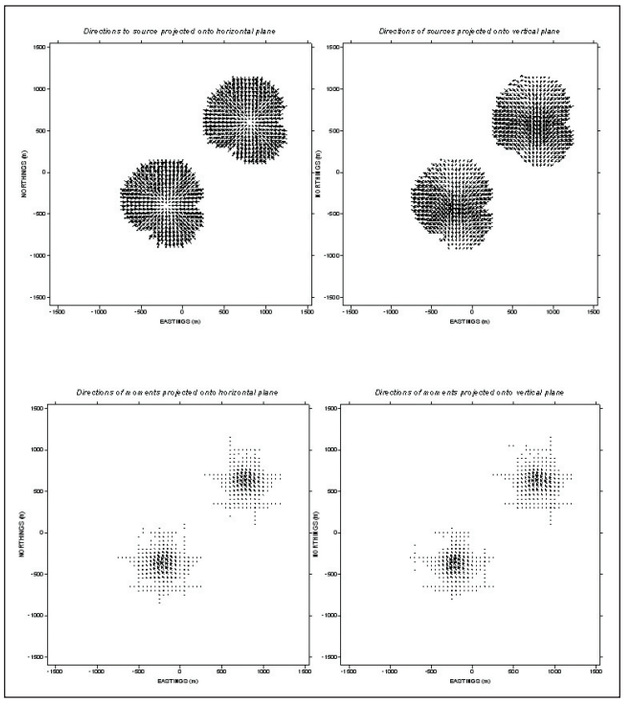

Fig. 1. Projections of $\hat{\mathbf{n}}$ (direction from the source) and $\mu\hat{\mathbf{m}}$ (magnitude of magnetic moment × direction of the moment) onto horizontal and vertical planes.

Recently, Heath et al. (2003) have examined a number of inversion schemes for the magnetic gradient tensor. Inversion schemes are generally iterative forward models, searching for a minimum difference between observation and model response. A Monte Carlo approach was found to have the benefit of probing the solution-space as broadly as possible, thus avoiding local minima, but it is inefficient. The Amoeba optimisation method (Downhill Simplex) was also tried and, while efficient, it runs the risk of becoming trapped in local minima especially when fitting more than a few parameters.

The authors suggest running the Amoeba a number of times beginning with different initial parameters thus effectively combining the Monte Carlo and Amoeba approaches to optimise efficiency and ensure the global minimum is found.

In most geophysical surveys, anomalies are rarely found in isolation, thus somewhat compromising dipole or other geometrical model inversion schemes. A more general scheme involves Euler deconvolution (Zhang et al., 2000). Although Zhang et al. (2000) developed Tensor Euler Deconvolution for gravity surveys, its extension to the magnetic case is obvious. This method has the advantage over those discussed by Heath et al. (2003) as the source geometry is entirely contained in a 'structural index' that varies from 0 for a uniformly magnetized extensive stratum, such as a sill (a magnetic annihilator), to 3 for an isolated dipole, such as IOCG deposits (at a distance) or UXO. (Note that higher indices are possible, e.g., 4 for a quadrupole, but these are rare in nature.) Once the geometry of a source is determined, its location and magnetic properties can be further constrained by studying the eigenvalues and eigenvectors of the magnetic gradient tensor at judiciously selected points near the source. It turns out that surprisingly few tensor observations are required to furnish all the determinable information about a source, i.e., notwithstanding fundamental non-uniqueness that prevents, for example, the determination of the radius of spherical sources, the along-strike component of magnetization of bodies with significant strike extent, or separately determining the dip and magnetic inclination of dyke-like bodies.

PHILOSOPHY OF MEASURING GRADIENTS

The most appropriate sensors for gradient measurements are SQUIDs – (see Foley et al., 1999 and Foley and Leslie, 1998). SQUIDs detect minute changes of flux threading a superconducting loop. They are therefore variometers rather than magnetometers, but they are vector sensors since only changes perpendicular to the loop are detected. So-called 'high-temperature superconducting' SQUIDs, or HTS SQUIDs, operate at liquid-nitrogen temperatures, overcoming the logistical problems of handling liquid helium required by 'low-temperature' SQUIDs. The response of a SQUID sensor to a magnetic field can either be measured using an analogue flux-locked loop (FLL), where an integral of the measured flux is fed back to the SQUID to cancel the sensed field, or via flux-counting systems, which count flux quanta as they enter or leave the SQUID loop. The sensitivity of HTS SQUIDs is of the order of 10–100 fT (10–100×10^{-6} nT, i.e., 1 fT = 10^{-6} nT).

It has been shown that a gradiometer sensitivity of 0.01 nT/m is sufficient to detect even weak magnetic contrasts at 500 m height (Bick et al., 2004a). To adapt SQUID sensors to measure magnetic gradients we initially considered using discrete SQUIDs on a baseline of ~10 cm. The outputs of the SQUIDs would be electronically differenced, effectively providing the magnetic gradient between the sensors. In this way, axial or transverse gradients can be measured depending on the sensor configuration. A disadvantage of this 'difference method' is that the dynamic range for each SQUID sensor must at least equal twice the Earth's

field, which is difficult to realise with a conventional scheme. If a flux-counting feedback scheme is used with a HTS SQUID, the SQUID's low-frequency noise performance is typically degraded because of thermal agitation of the flux vortices lying within the SQUID loop. In either technique, if the HTS SQUID electronics lose lock, the SQUID will be exposed to Earth's field; flux will enter the SQUID loop and typically lead to an increase in SQUID noise. Thus it has proved far more advantageous to measure the true gradient by coupling a single SQUID to counter-wound pick-up loops. This set-up allows the SQUID to be shielded and to effectively only sense a small field resulting from the difference in Meissner screening currents generated in the pick-up loops. Moreover, imperfection of alignment or differences in the size of the pick-up loops introduces a signal proportional to the field component quasi-parallel to the loop axes. Hence this configuration can yield both tensor and vector components. Of course the vector components are afflicted with the extreme orientation sensitivity as described above, but even so, they allow the ambiguity of the tensor analysis for dipoles to be solved independently of any a priori knowledge of the location of the source. In fact, even the signs of the (anomalous) vector components are sufficient to yield a unique solution to the tensor inversion of dipole gradients.

GRADIOMETER PRINCIPLE AND SYSTEM DESIGN

Based on the theory developed by Tilbrook (2004), and as described also at <http://www.tip.csiro.au/IMP/SmartMeasure/ASC2002_GETMAG_Presentation.pdf>, three rotating axial gradiometers in an umbrella configuration, as shown in Figure 2, are sufficient to obtain the full first-order magnetic gradient tensor. The initial phase of this research program was to test the GETMAG rotating gradiometer concept, and it was considered sufficient to use a prototype system consisting of one axial gradiometer that could be manually rotated about the intrinsic z'-axis, i.e., the z-axis rotated to 45° from the normal, through eight discrete fixed positions spaced 45° apart (Figure 3). The intrinsic z'-axis is orientated at 45° with respect to the horizon in accordance with theory. To obtain the full magnetic gradient tensor, the system could be swung through 120° increments around the vertical z-axis, with an accuracy of better than 0.1°. A sequence of 3 × 8 measurements is necessary to record the magnetic gradient tensor, B_{ij}, at any one location.

The axial SQUID gradiometer operates in liquid nitrogen at 77 K. A detailed description of the axial gradiometer is given in Bick et al. (2004b). The gradiometer measures the first derivative of the magnetic field, $\partial B_i/\partial j$, $i = j$, $i, j = \{x', y', z'\}$. It consists of a directly coupled SQUID magnetometer, a flexible superconducting flux transformer, and a superconducting shield (Figures 4 and 5). The flexible flux transformer is patterned in a single layer of 700 nm thick superconducting $YBa_2Cu_3O_{7-x}$ (YBCO) film on a 10 × 85 mm² flexible Hastelloy tape with a thickness of ~ 70 μm (Figure 5a). The SQUID is hermetically sealed in a heater capsule to enable heating above its critical temperature for removal of trapped flux when required.

The SQUID, transformer, and shield are assembled in the holder shown in Figure 5b, which was fixed to the base of a radio-frequency-shielded glass Dewar flask. The Dewar flask was mounted on a purpose-built manually rotated holder, which provided a locking mechanism for each of the eight axial and three orthogonal positions. The Dewar flask was double-shielded to ensure sufficient exclusion of radio-frequency fields. The Dewar flask holding time is more than 8 hours in the operating position (i.e., 45° tilt with respect to the horizon) under normal field trial conditions.

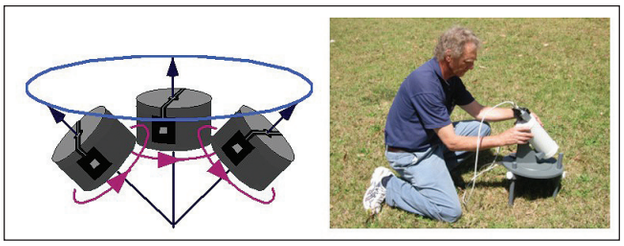

Fig. 2. (Left) Schematic of the GETMAG sensor configuration with the three rotating sensors in an umbrella configuration. (Right) the prototype consists of a single sensor, which is swung around through 120° increments about the vertical axis.

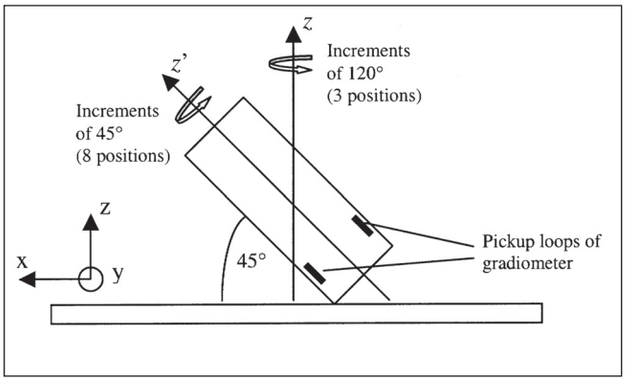

Fig. 3. A single axial gradiometer drum is rotated around its intrinsic z'-axis through 8 fixed positions in 45° increments. To obtain the full gradient tensor, the drum is rotated around the instrument's z-axis through 3 fixed positions in 120° increments resulting in 3 × 8 measurements.

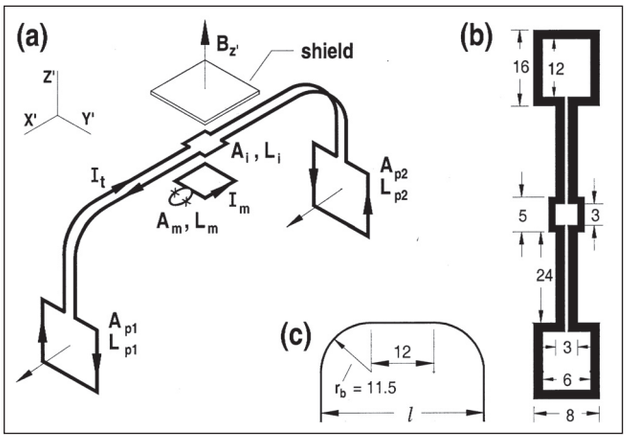

Fig. 4. (a) geometrical design of the pick-up loops comprising a flexible superconducting flux transformer on a Hastelloy substrate, shield, and SQUID all of which operate in liquid nitrogen at 77K. (b) and (c) Dimensions of the flux transformer. Dimensions are in mm (from Bick et al., 2004).

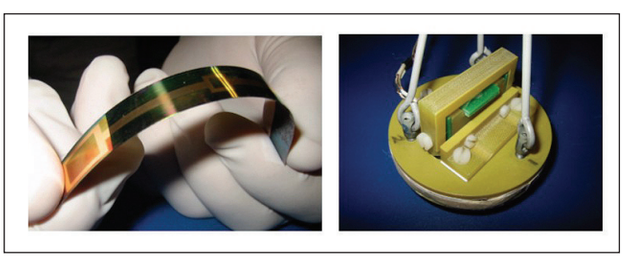

Fig. 5. (a) The flexible superconducting flux transformer on a 70 μm thin Hastelloy substrate (see Figure 4). (b) Holder for the SQUID, flux transformer, and shield. Three rods were used to change the distance and tilt between shield and SQUID from outside the liquid nitrogen Dewar flask, by means of differential screws.

The SQUID was connected to commercial DC electronics (Star Electronics: preamplifier PFL-100 and control electronics PCI-100) without flux-bias reversal. Additional purpose-built electronics were used to filter and collect the recorded data. These electronics were mounted on a purpose-built cart, which provided mobility of the system during the trial. Specially developed software (GETMAG Sampler V.2.0) allowed operators to extract, save, and analyse the magnetic gradient tensor and field from the data collected from the SQUID sensor. A block diagram of the GETMAG system is shown in Figure 6.

TALLAWANG FIELD TRIAL

The Tallawang magnetite skarn is situated 18 km north of Gulgong, NSW, along the western margin of the Gulgong Granite (Figure 7), which was intruded during the waning stages of the Kanimblan Orogeny in the Late Carboniferous. The deposit is roughly tabular, striking NNW and dipping steeply to the west. In detail, the magnetite occurs in lenses thought to reflect replacement of a tightly folded host rock sequence (Tucklan Beds), and is additionally complicated by transverse faulting, causing east-west displacement of the magnetite zones (Weekes, 1995).

The magnetite body is well delineated by numerous drill holes and the rock magnetic properties of the magnetite have been well characterised. The strongest samples possessed susceptibility of 3.8 SI (0.3 cgs) and remanence of 40 $A.m^{-1}$, yielding Koenigsberger ratios (Qs) of about 0.2–0.5. The mean direction of the remanence is WNW and steeply up. This direction may be the result of a dominant viscous remanent magnetization (VRM) in the direction of the recent geomagnetic field, and a reversed mid-Carboniferous component, dating from the time that the Gulgong Granite was intruded. The effective magnetization, projected onto a vertical plane perpendicular to strike, is directed steeply upward.

A high resolution TMI gradiometer survey using two Caesium-vapour magnetometers separated vertically by 1 m was undertaken in parallel to the deployment of GETMAG. Continuous readings were taken along east-west grid lines spaced 10 m apart. Although a peg grid was laid out, principally for GETMAG, a GPS system was used to automatically locate the TMI gradiometer readings. The purpose of the survey was to allow the calculation of the tensor gradients from the TMI and also to compare the measured TMI vertical gradient with the vertical gradients of the tensor, which were calculated from the TMI. The TMI was taken as the

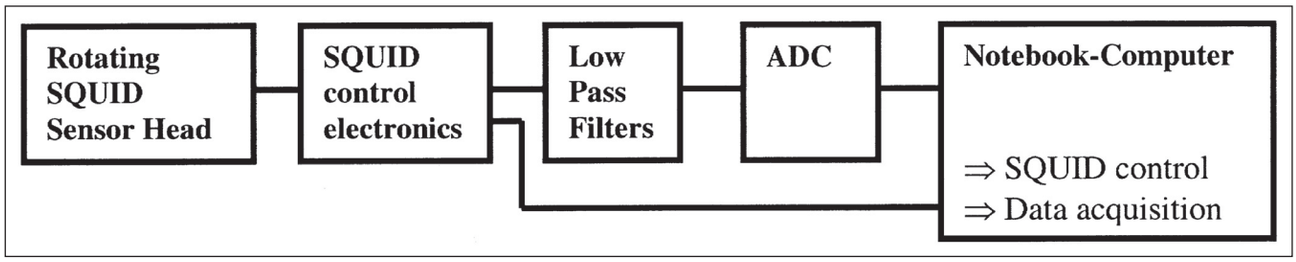

Fig. 6. Block diagram of GETMAG system including the manually rotated SQUID gradiometer.

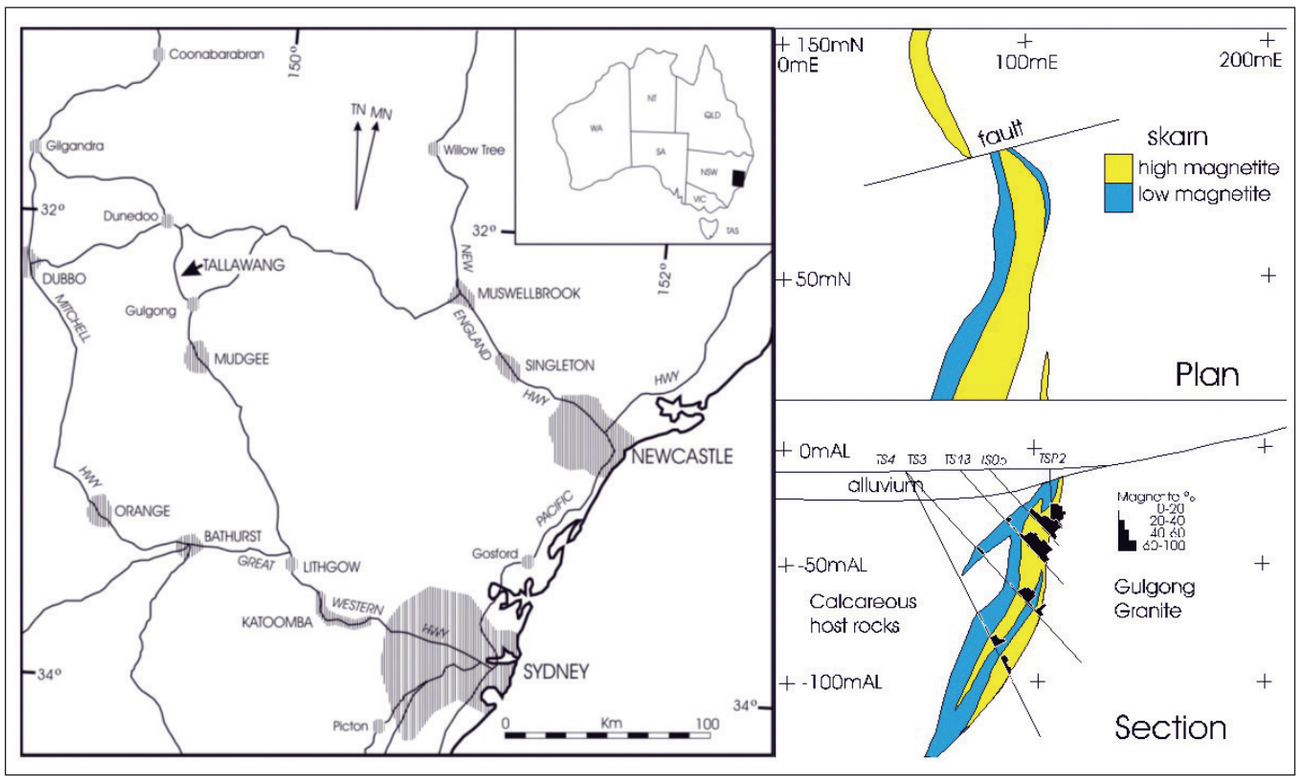

Fig. 7. Location and geological map and section based on extensive drilling and analysis of the Tallawang South deposits. The magnetite content of samples taken from the drill holes is also shown. The maximum measured susceptibility (k = 3.8 SI) corresponds to 60–70% by volume of coarse-grained magnetically soft magnetite, which is typical of the low-stress hydrothermal environment of the Tallawang skarn mineralisation.

mean of the upward- and downward-continued TMI surveys from the lower and upper Cs-vapour magnetometers. The height above the ground for the continuation was 1 m, to agree with the height at which GETMAG operates.

Three profiles crossing the target were selected for GETMAG measurements, the 50mN, 60mN, and 120mN lines (see Figure 8) with station spacings of 10 m, reducing to 5 m near the peak of the anomaly.

The Tallawang site and white survey pegs marking the 50mN line are shown in Figure 10. At every station, the gradiometer platform was levelled using an integrated spirit level. The intrinsic y-axis of the system pointed east and was aligned by adjusting the beam of a laser pointer to a line-station at ≥10 m distance. The laser pointer was attached to the horizontal gradiometer platform only for the alignment procedure and was removed for each measurement. The residual misalignment to the grid was estimated to be less than 1°.

The tensor gradient was recorded by manually rotating the gradiometer as described previously. For every measurement, 128 samples at a sampling rate of 200 samples/sec were taken, corresponding to a recording time of 640 ms or a measurement bandwidth of DC to ~1.56 Hz. An anti-aliasing second-order, low-pass filter at 20 Hz was applied. A total of 8 × 3 measurements were necessary to determine the full gradient tensor. From the 24 measurements, the tensor was calculated automatically by the GETMAG software using the calibration coefficients determined in the laboratory. At every station, at least two full tensor recordings were taken to check for consistency. In addition, a consistency check at a known station (50N, 0E) was performed every morning, which showed reproducible results with and without an introduced localized magnetic anomaly generated by a small magnetic dipole placed at a known distance from this station. Figures 10 and 11 show the operation of the GETMAG system during the field trial. When fully developed the system will be automatically rotated, allowing about 30 full tensor measurements per second.

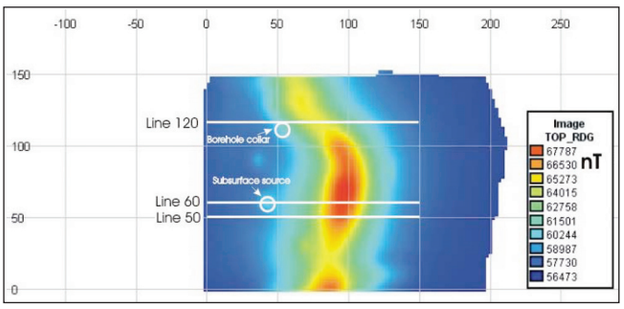

Fig. 8. Tallawang TMI survey [nT] and the three (white) lines along which tensor gradient measurements were performed with the rotating GETMAG gradiometer. Grid north is 340° True.

TMI results and comparison with GETMAG results

The TMI image and images of the main tensor components perpendicular to strike were produced using in-house software and *ModelVision* software, and are shown in Figures 8 and 9. The TMI anomaly has an amplitude of 12 000 nT and is reasonably symmetric, reflecting the steep-upward magnetization. As mentioned above, the measured remanent magnetization direction is to the WNW and steep-up. In addition, any induced magnetization is likely to be deflected into the plane of the lenses because of effects of self-demagnetization, and the component along strike will not contribute to the anomaly. Therefore, the effective induced magnetization is also steep-up like the remanent magnetization.

Figure 12 shows for each survey line comparisons of the tensor elements measured by GETMAG with those calculated from the TMI data. There is an excellent quantitative agreement between the pairs of profiles. This demonstrates the accuracy of the GETMAG calibration and confirms the algorithm developed to calculate gradient tensor elements from a densely sampled TMI survey.

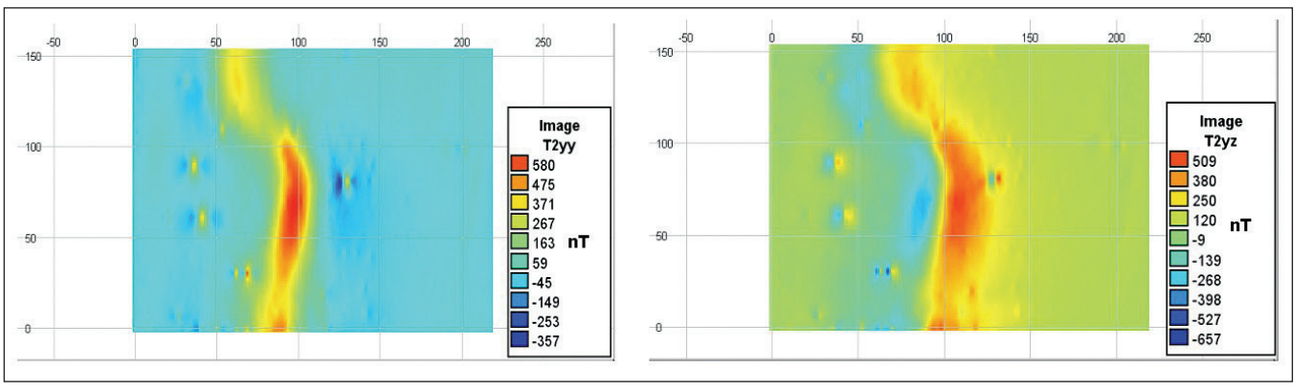

Fig. 9. Calculated B_{yy} and B_{yz} (easterly and vertical gradient of grid E components) images of Tallawang South magnetite skarn anomaly.

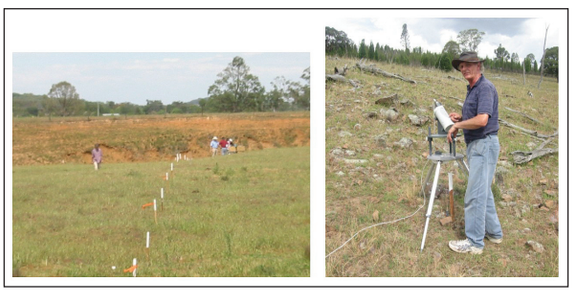

Fig. 10. 50mN line at Tallawang South (looking west) and the GETMAG rotating sensor head including the liquid nitrogen Dewar flask, which is mounted on a tripod at a 45° angle (looking east, up the slope of the Gulgong Granite).

Fig. 11. Operating the GETMAG system via a notebook computer on a trolley, which carried control electronics, filters, and battery packs.

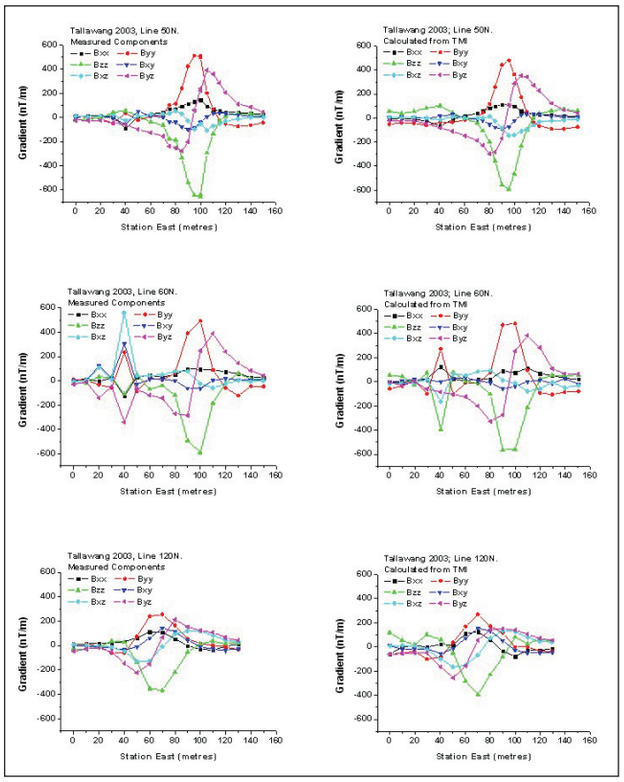

Fig. 12. Comparison of GETMAG and TMI derived tensors for Lines 50mN, 60mN, and 120mN.

The TMI calculated elements are slightly smoother, reflecting loss of fine detail, because of the spatial averaging that is inherent in the gridding of single component data and in the Fourier domain processing that yields the tensor elements. We emphasise that to determine the gradient tensors from TMI, a densely sampled TMI survey that adequately covers the whole anomaly is required, whereas with GETMAG the same information is obtained from only a few stations. This will be demonstrated in the following sections.

Data Analysis: Inversion of Tallawang Tensor Data

GETMAG data from the three profiles over the Tallawang deposit were analysed using inversion algorithms developed for thin-sheet and thick-sheet models. Each tensor measurement provides an estimate of the local strike, provided the source is approximately two-dimensional. This assumption is testable. Only stations for which the intermediate eigenvalue (λ_2) has a much smaller absolute value than the other two eigenvalues (λ_1 and λ_3), and for which the corresponding eigenvector is sub-horizontal, should be used for estimating the strike. When the strike is determined, the tensors at each station are transformed into a co-ordinate system with x (say) along the profile, y parallel to strike, and z down. Then all elements that involve y become small relative to the range of values exhibited by B_{xx}, B_{xz}, and B_{zz}. In addition, $B_{xx} \approx -B_{zz}$.

It can be shown that for 2D sources the eigenvalues of the tensor are:

$$\lambda = \pm\sqrt{\left[\left(B_{xx}\right)^2 + \left(B_{xz}\right)^2\right]} = \pm\sqrt{\left[\left(B_{zz}\right)^2 + \left(B_{xz}\right)^2\right]}. \qquad (17)$$

The eigenvalues are rotational invariants of the tensor and are independent of the magnetization direction of the source. A unimodal curve of $|\lambda|$ versus x indicates a relatively thin sheet. The peak of the eigenvalue, which is equivalent to the 2D total gradient or analytic signal amplitude, indicates the approximate centre x_0 of the sheet. The half-width at half-maximum (HWHM) of the eigenvalue curve provides an estimate of the depth h of the sheet. The magnetization-thickness (Jt) product can then be estimated from the maximum eigenvalue and the depth. The signs of the components (J_x, J_z) of the effective magnetization are indicated by the signs of B_{xx}, B_{xz} in the vicinity of the eigenvalue peak. This determines the quadrant in which the effective magnetization lies.

Tensor Euler Deconvolution

A convenient method to visualise and analyse a survey of tensor measurements is Tensor Euler Deconvolution (Zhang et al., 2000). Following Blakely (1996), homogeneous functions are defined as those that satisfy Euler's equation,

$$\hat{\mathbf{r}} \cdot \nabla f = -nf, \qquad (18)$$

where n is called the Euler structural index or attenuation rate. Taking derivatives,

$$\frac{\partial}{\partial x}\left[\hat{\mathbf{r}} \cdot \nabla f\right] = \frac{\partial}{\partial x} f + \hat{\mathbf{r}} \cdot \nabla \frac{\partial}{\partial x} f = -n \frac{\partial}{\partial x} f, \qquad (19)$$

and re-arranging,

$$\hat{\mathbf{r}} \cdot \nabla \frac{\partial}{\partial x} f = -(n+1) \frac{\partial}{\partial x} f, \qquad (20)$$

it is shown that the derivative of a function also satisfies the Euler equation, albeit with a higher order index. Since $1/r$ is a homogeneous function, the potential field of a monopole satisfies Euler's equation. Therefore, multipole distributions being functions of spatial gradients of $1/r$ must also obey Euler's equation. Euler deconvolution as normally applied to TMI surveys may be expressed as:

$$x\frac{\partial B}{\partial x} + y\frac{\partial B}{\partial y} + z\frac{\partial B}{\partial z} = -nB, \qquad (21)$$

where B is the anomalous field. The same relationships apply to gradients of components,

$$x\frac{\partial B_x}{\partial x} + y\frac{\partial B_x}{\partial y} + z\frac{\partial B_x}{\partial z} = -nB_x, \qquad (22)$$

and by extension, to the gradient tensor, and allowing for an arbitrary origin,

$$\begin{bmatrix} \frac{\partial B_x}{\partial x} & \frac{\partial B_x}{\partial y} & \frac{\partial B_x}{\partial z} \\ \frac{\partial B_y}{\partial x} & \frac{\partial B_y}{\partial y} & \frac{\partial B_y}{\partial z} \\ \frac{\partial B_z}{\partial x} & \frac{\partial B_z}{\partial y} & \frac{\partial B_z}{\partial z} \end{bmatrix} \begin{bmatrix} x - x_0 \\ y - y_0 \\ z - z_0 \end{bmatrix} = -n \begin{bmatrix} B_x \\ B_y \\ B_z \end{bmatrix}. \qquad (23)$$

Since there are four unknowns, n, x, y, and z, at least two tensors are required for each source to solve in a least-squares fashion. In practice, as many tensors are combined as possible until the least-squares error increases. The application of Tensor Euler Deconvolution to the tensors derived from the Tallawang TMI

survey (Figure 13) demonstrates the potential of tensor surveys to yield both location and structural index of sources. It should be emphasised here that the calculation of tensor components from the TMI at Tallawang has been successful because the structure is essentially 2D and the survey was approximately perpendicular to strike. This assured that aliasing is minimised. In general this cannot be guaranteed, especially where sources of differing geometries are encountered.

In Figure 13, the background is dominated by very low indices, corresponding to uniformly magnetized strata (approaching a magnetic annihilator, which has no external magnetic expression). The skarn deposit is mostly a dyke-like body whose top is about 10 m deep with an index close to unity, with fingers of higher index geometry (up to about 2.5) at a greater depth of about 30 m. These apophyses are most probably fresh, unweathered magnetite with a significant magnetization contrast to the mantle of weathered skarn.

This demonstrates the power of Tensor Euler Deconvolution in 3D mapping of magnetic sources. Where resolution permits, the process may be applied directly to TMI.

DISCUSSION AND CONCLUSIONS

The GETMAG project has resulted in the invention of a new axial gradiometer based on the use of high-temperature superconducting flexible tape pick-up loops coupled to a SQUID. The use of rotating sensors reduced the number of sensors required to measure the full nine components of the magnetic tensor. Algorithms to extract these data from the sensor outputs and various data interpretation and analysis software have also been developed.

The gradiometer is operated at the liquid nitrogen temperature of -196°C that provides significant logistical advantages over liquid helium-cooled systems. The concept has been verified with a manual rotating system. As the final airborne system will be operated at an anticipated rotation frequency of ~30 Hz, low-frequency noise can be reduced using a simple suspension system. It is hoped to demonstrate this in the near future.

The field trial at Tallawang over a well-characterised magnetite target showed excellent agreement between the measured GETMAG gradient tensors and those calculated from the detailed TMI survey by Fourier filtering. This demonstrates the accuracy of the GETMAG calibration and confirms the Fourier filtering algorithm developed to calculate gradient tensor elements from a densely sampled TMI survey. The TMI calculated elements, however, are slightly smoother, reflecting loss of fine detail due to spatial averaging of the Fourier filter.

An important result from the Tallawang trial is the confirmation of our theoretical prediction that a densely sampled TMI survey covering the whole anomaly is required to calculate meaningful gradient tensors. Only in this way is it possible to retrieve the same information that is obtained by GETMAG from only a few stations.

Analysis of the GETMAG data from three profiles over the South Tallawang deposit confirmed that all the determinable parameters of dipping sheet-like sources could be reliably estimated from a limited number of tensor measurements, as few as 4–6. These parameters are the local strike (in principle determinable by a single station), the magnetization-thickness product, the depth, the thickness and magnetization separately if the sheet is not too thin and the effective magnetization intensity and direction of the equivalent vertical sheet. If the dip is known, the magnetization direction can be inferred. Conversely, if the magnetization direction is known, or can be assumed, the dip is determined. A change of strike between the northern and southern parts of the survey area enabled determination of the direction of magnetization in the deposit.

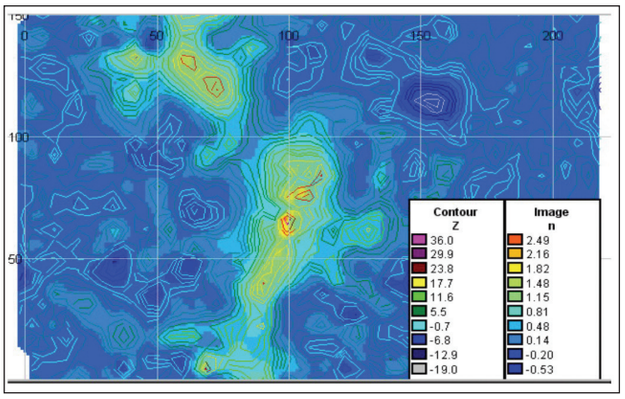

Fig. 13. Contours of depths to sources, z, and image of Euler structural index, n.

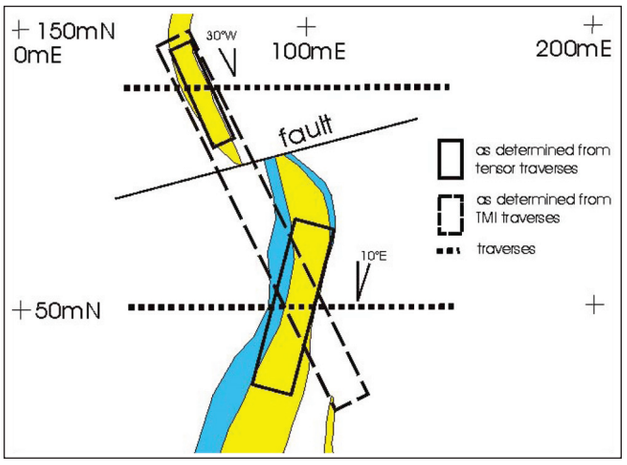

Fig. 14. Schematic diagram showing the difference between the inversion of two lines of tensor information and two lines of TMI data. Inversion of the TMI data would yield a poor representation of the geology whereas the change of strike direction is readily apparent in the tensor inversion.

The configuration of the GETMAG survey at Tallawang allowed a comparison of the information that could be obtained by the measurement of the gradient tensor and the TMI measurements along two profiles, separated by 50 m, one in the geological zone south of the fault and the other north of it (Figure 14). The GETMAG lines in the two geological domains indicated a distinct difference in the local strike and an offset in the source location that implies the existence of a structural break between them, and suggests the en-echelon pattern of the detailed geological map. On the other hand, TMI profiles along 55N and 120N registered highs over the magnetite lenses, without any indication of how these anomalies should be connected. Contouring or imaging software would simply join the peaks, yielding an erroneous strike and giving no indication of the geologically significant structural break between the zones. The separation of the profiles would be comparable to the line spacing of a very high resolution, low-level aeromagnetic survey.

The tensor components along a short segment of a survey line or drill hole are sufficient to determine the location and magnetic moment of a compact (quasi-dipolar) source uniquely. There is insufficient information in $\nabla(\Delta\mathbf{B}_m)$ (i.e., measurement of

TMI gradients in three orthogonal directions) to solve for these parameters. However, TMI and gradient tensor measurements should be seen as complementary, rather than competitive. As an example, measurement of the gradient tensor and the TMI anomaly, or a TMI gradient, at each point removes the ambiguity of dipole-tracking solutions. A magnetic tensor gradiometer sensor package could record field components (i.e., $\Delta\mathbf{B}$), as well as the gradients of these components, which would also allow direct determination of compact source location and moment.

Although the GETMAG project is aimed at developing an airborne tensor gradiometer for mineral exploration, other spin-off applications are evident. A ground-based version of the instrument would have applications in environmental and UXO surveys, as well as exploration and mine-site geophysics. A miniaturised version for down-hole use could greatly enhance the utility of down-hole magnetics, which is currently restricted to investigation of highly magnetic ore bodies. A combined tensor/vector magnetometer package would allow the remote determination of in situ magnetic properties of sources from the surface or subsurface, using natural geomagnetic variations, without the alignment problems that afflict the differential vector magnetometer method (Clark, 1997; Clark et al., 1998).

ACKNOWLEDGEMENTS

Our colleagues in CSIRO Industrial Physics who have contributed to the success of the GETMAG project include Rex Binks, Canice Cheung, Jia Du, Rajan Gnanarajan, Nigel Hoschke, Peter Issacs, Simon Lam, Emma Mitchell, Chris Sharman, Peter Sullivan, and Robert Thorn. Mineral exploration companies that have contributed include BHP Innovation, De Beers Australia, Normandy Exploration, MIM Exploration (now Xstrata) and WMC Exploration. We gratefully acknowledge the contributions of all these participants. Drs Peter Milligan and Tony Meixner are thanked for their careful reviews of the paper and the resulting clarification of some potentially confusing sections.

REFERENCES

Bick, M., Clark, D.A., Foley, C.P., Leslie, K.E., Schmidt, P.W., and Tilbrook, D.L., 2004a, *GETMAG Phase 1 Completion*: CSIRO Confidential Report to Sponsors.

Bick, M., Leslie, K.E., Binks, R.A., Tilbrook D.L., Lam, S.K.H., Gnanarajan, S., Du, J., and Foley, C.P., 2004b, Axial high-T_c superconducting gradiometer with a flexible flux transformer, *Appl. Phys. Lett*., **84**, 5347–5349.

Blakely, R.J., 1996, *Potential theory in gravity and magnetic applications*: Cambridge University Press, 441pp.

Christensen, A., and Rajagopalan, S., 2000, The magnetic vector and gradient tensor in mineral and oil exploration: *Preview,* **84**, 77.

Clark, D.A., 1997, Theory of Differential Vector Magnetometry – a new method for remote determination of in situ magnetic properties and improved drill targeting: *Exploration and Mining, North Ryde, **Report 395R***, 19 pp.

Clark, D.A., Schmidt, P.W., Coward, D.A., and Huddleston, M.P., 1998, Remote determination of magnetic properties and improved drill targeting of magnetic anomaly sources by Differential Vector Magnetometry (DVM): *Exploration Geophysics*, **29**, 312–319.

Emerson, D.W., Clark, D.A., and Saul, S.J., 1985, Magnetic exploration models incorporating remanence, demagnetisation and anisotropy: HP 41C handheld computer algorithms: *Exploration Geophysics*, **16**, 1–122.

Foley, C.P., and Leslie, K.E., 1998, Potential use of High Tc SQUIDs for Airborne electromagnetics: *Exploration Geophysics,* **29**, 30–34.

Foley, C.P., Leslie, K.E., Binks, R., Lewis, C., Murray, W., Sloggett, G.J., Lam, S., Sankrithyan, B., Savvides, N., Katzaros, A., Muller, K.H., Mitchell, E.E., Pollock, J., Lee, J., Dart, D.L., Barrow, R.R., Asten, M., Maddever, A., Panjkovic, G., Downey, M., Hoffman C., and Turner, R., 1999, Field Trials using HTS SQUID Magnetometers for Ground-based and Airborne Geophysical Applications: *IEEE Trans. Appl. Supercond*., **9**, 3786–3792.

Frahm, C.P., 1972, Inversion of the magnetic field gradient equation for a magnetic dipole field: *NCSL Informal Report,* 135–72.

Heath, P., Heinson, G., and Greenhalgh, S., 2003, Some comments on potential field tensor data: *Exploration Geophysics*, **34**, 57–62.

Schmidt, P.W., and Clark, D.A., 2000, Advantages of measuring the magnetic gradient tensor: *Preview*, **85**, 26–30.

Tilbrook, D.L., 2004, The design of a new concept HTSC axial gradiometer: *Physica C*, **407**, 1–9.

Vrba, J., 1996, SQUID gradiometers in real environments: in Weinstock, H. (ed.), *SQUID Sensors: Fundamentals and Applications*, *Kluwer Academic*, p117.

Weekes, G., 1995, Tallawang South magnetite deposit; report on geological investigations 1993 to 1995, Vols. I and II: *Commercial Minerals Limited*, Report **19959**.

Wilson, H., 1985, Analysis of the magnetic gradient tensor: *Defence Research Establishment Pacific: Canada Technical Memorandum,* **85-13**, 47.

Wynn, W.M., Frahm, C.P., Carroll, P.J., Clark, R.H., Wellhoner, J., and Wynn, M.J., 1975, Advanced superconducting gradiometer/magnetometer arrays and a novel signal processing technique: *IEEE Trans. Mag.,* **MAG-11**, 701–707.

Zhang, C., Mushayandevu, M.F., Reid, A.B., Fairhead, J.D., and Odegard, M.E., 2000, Euler deconvolution of gravity tensor gradient data: *Geophysics*, **65**, 512–520.